Optical forces near a plasmonic nanostructure

Vassilios Yannopapas*
Department of Materials Science, University of Patras, GR-26504 Patras, Greece
(Received 14 April 2008; revised manuscript received 10 June 2008; published 10 July 2008)

We present a rigourous theory for the calculation of the optical trapping force exerted on a particle placed near an externally illuminated periodic monolayer of spheres. The electromagnetic-field incident on the particle is calculated by taking into account all the multiple-scattering processes taking place within the monolayer. Having calculated the incident and scattered electromagnetic fields from the particle, we integrate the corresponding Maxwell stress tensor over the surface of the body in order to find the exerted optical force. For a complete treatment of the optical trapping problem, we also calculate the van der Waals–Casimir force exerted on the particle from the monolayer, namely, we calculate the cross-spectral correlation functions of the vacuum electromagnetic-field fluctuations by means of the fluctuation-dissipation theorem and a multiple-scattering Green's tensor formalism. Having calculated the fluctuating electromagnetic fields entering the Maxwell stress tensor, we obtain the van der Waals–Casimir force. The formalism is applied to the case of a small dielectric particle placed in proximity to an illuminated monolayer of close-packed metallic nanospheres in various transmission geometries. It is found that, under strong laser intensities, the optical force can trap the particle near the plane of the spheres due to the gradient of the optical near field.

DOI: 10.1103/PhysRevB.78.045412 PACS number(s): 78.67.Bf, 42.50.Wk, 37.10.Jk, 87.80.Cc

I. INTRODUCTION

Since the first demonstration of trapping of neutral particles by optical means[1,2] and, especially, by the optical tweezing technique,[3–5] there has been a wide application of the optical forces in atomic physics, biology, and chemistry.[6] A focused beam, such as those used in the optical tweezing technique, exerts a gradient force on a particle toward the focal point allowing for the transfer of the particle to a prescribed location. Apart from a focused beam, optical manipulation of particles takes place by other gradient fields such as a standing wave formed by two counter-propagating beams[7] or an exponentially decaying near field close to a planar surface.[8–10] In the presence of many particles, a gradient field may even induce the formation of ordered arrays[11–18] or stabilize/dismantle colloidal structures.[19] The use of complex beams such as Bessel,[20] Laguerre-Gaussian,[21] and helical Laguerre-Gaussian beams[22] (as well as beams created by programmable holograms),[23–26] enable (in principle) the realization of tailor made two-dimensional (2D) and three-dimensional (3D) optical potential landscapes.

Another route for creating optical traps for neutral particles is to make use of the large gradient (near) fields generated by the scattering of light on microstructured surfaces[27] and photonic-crystal based structures.[28–30] The advantage of these optical potential landscapes over the holographic ones lies in the ability to trap large numbers of particles. The optical forces exerted on the trapped particles can be further strengthened by tuning the frequency of incident light with possible inherent resonances of the trapped particles[31] such as surface plasmons.[32,33]

Based on this context, we study the optical forces exerted on a nanoparticle near a plasmonic nanostructure, namely, near a monolayer of close-packed plasmonic (metallic) nanospheres. This nanostructure can induce strong optical forces on a neighboring neutral test particle due to the near-field landscape generated by light incident on the monolayer. Under suitable laser power and frequency, the optical forces can overcome the van der Waals–Casimir (VDWC) forces and the thermal noise, leading to local confinement of the particle. Under plane-wave illumination, the electromagnetic (EM) field reaching the test particle is calculated by the layer-multiple-scattering (LMS) method.[34] The corresponding EM force is obtained by integrating the Maxwell stress tensor over the surface of the test particle. The calculated optical forces are compared against the VDWC forces exerted on the test particle from the nanostructure. These forces are calculated by a fluctuational electrodynamics multiple-scattering approach for macroscopic bodies. The paper is organized as follows: Sec. II presents the theory for the calculation of the optical force acting on small test particle in the vicinity of a nanostructure. Sec. III briefly presents the theory for the calculation of the VDWC force. Sec. IV presents the results for the optical and VDWC force acting on small dielectric sphere near a monolayer of plasmonic nanospheres and Sec. V concludes the paper.

II. OPTICAL FORCE

A. Scattering by a single scatterer

In this subsection we present a brief summary of the solution to the problem of EM scattering from a single sphere (Mie scattering theory[35,36]). We consider a sphere of radius S, with its center at the origin of coordinates, and we assume that its electric permittivity ϵ_s and/or magnetic permeability μ_s are different from those, ϵ_h and μ_h of the surrounding homogeneous medium. We also consider a harmonic EM wave of angular frequency ω, which is described by its electric-field component,

$$\mathbf{E}^0(\mathbf{r},t) = \mathrm{Re}[\mathbf{E}(\mathbf{r})\exp(-\mathrm{i}\omega t)], \tag{1}$$

where

$$\mathbf{E}^0(\mathbf{r}) = \mathbf{E}_0(\mathbf{q})\exp(i\mathbf{q}\cdot\mathbf{r}). \tag{2}$$

If the above wave is incident on the sphere, it is convenient to express it as a sum of vector spherical waves which are incident on the sphere,[35]

$$\mathbf{E}^0(\mathbf{r}) = \sum_{l=1}^{\infty}\sum_{m=-l}^{l}\left\{a^0_{Hlm} j_l(qr)\mathbf{X}_{lm}(\hat{\mathbf{r}}) + a^0_{Elm}\frac{i}{q}\nabla \times [j_l(qr)\mathbf{X}_{lm}(\hat{\mathbf{r}})]\right\}, \tag{3}$$

where $q=\sqrt{\epsilon_h\mu_h}\omega/c$. $\mathbf{X}_{lm}(\hat{\mathbf{r}})$ are the so-called vector spherical harmonics[35] and j_l are the spherical Bessel functions. The corresponding magnetic field can be readily obtained from $\mathbf{E}^0(\mathbf{r})$ using Maxwell equations.[35] The expansion coefficients a^0_{Plm} $(P=E,H)$ are given elsewhere.[35]

The wave of Eq. (3) will be scattered off the sphere and the scattered electric field is provided by

$$\mathbf{E}^+(\mathbf{r}) = \sum_{l=1}^{\infty}\sum_{m=-l}^{l}\left\{a^+_{Hlm} h^+_l(qr)\mathbf{X}_{lm}(\hat{\mathbf{r}}) + a^+_{Elm}\frac{i}{q}\nabla \times [h^+_l(qr)\mathbf{X}_{lm}(\hat{\mathbf{r}})]\right\}, \tag{4}$$

where h^+_l are the spherical Hankel functions.

By applying the requirement that the tangential components of $\mathbf{E}$ and $\mathbf{H}$ be continuous at the surface of the scatterer, we obtain a relation between the expansion coefficients of the incident and the scattered field as follows:

$$a^+_{Plm} = \sum_{P'l'm'} T_{Plm;P'l'm'} a^0_{P'l'm'}, \tag{5}$$

where $T_{Plm;P'l'm'}$ are the elements of the so-called scattering transition T matrix.[36] Eq. (5) is valid for any shape of scatterer; for spherically symmetric scatterers, each spherical wave scatters independently from all others, which leads to a transition T matrix, which does not depend on m and is diagonal in l, i.e., $T_{Plm;P'l'm'}=T_{Plm}\delta_{Plm;P'l'm'}$. Analytic expressions are given elsewhere.[36]

B. Maxwell stress tensor and EM force

The time-averaged electromagnetic force acting on a sphere when an incident plane wave [such as that of Eq. (1)] impinges on the sphere, is given by the integral of the Maxwell stress tensor over the surface A of the sphere,

$$\langle F_i\rangle_t = \int_A \sum_j \langle T_{ij}\rangle_t n_j dS, \tag{6}$$

where $\langle..\rangle_t$ denotes the time average, $\mathbf{n}$ is the normal vector at the surface surrounding the object, and $i,j=x,y,z$. The components of the Maxwell stress tensor $\langle T_{ij}\rangle_t$ are given by

$$\langle T_{ij}\rangle_t = \epsilon_h\epsilon_0\langle E_i(\mathbf{r},t)E_j(\mathbf{r},t)\rangle_t + \mu_h\mu_0\langle H_i(\mathbf{r},t)H_j(\mathbf{r},t)\rangle_t - \frac{1}{2}\delta_{ij}\left[\epsilon_h\epsilon_0\sum_{i'}\langle E_{i'}(\mathbf{r},t)E_{i'}(\mathbf{r},t)\rangle_t + \mu_h\mu_0\sum_{i'}\langle H_{i'}(\mathbf{r},t)H_{i'}(\mathbf{r},t)\rangle_t\right], \tag{7}$$

where δ_{ij} is the Kronecker symbol, and ϵ_0 and μ_0 are the electric permittivity and magnetic permeability of vacuum, respectively. The field appearing in Eq. (7) is the total field outside the sphere, i.e., the sum of the incident and scattered fields: $\mathbf{E}(\mathbf{r})=\mathbf{E}^{\text{out}}(\mathbf{r})=\mathbf{E}^0(\mathbf{r})+\mathbf{E}^+(\mathbf{r})$, where $\mathbf{E}^0(\mathbf{r})$ and $\mathbf{E}^+(\mathbf{r})$ are given by Eqs. (3) and (4), respectively. By substituting Eqs. (3) and (4) into Eq. (7) and by performing the surface integration analytically, we obtain a final formula for the EM force. Explicit relations for the EM force can be found elsewhere.[37,38]

C. EM field near a plane of spheres

Let us consider a sphere placed at a distance h from the right side of a monolayer (plane) of spheres. We assume that the sphere is small enough so that it would not disturb significantly the EM field near the plane of spheres when the latter is illuminated by a plane wave. We consider that the plane of spheres is placed at $z=0$ and the spheres are centered on the sites $\mathbf{R}_n$ of a given 2D lattice. We define the 2D reciprocal vectors as $\mathbf{g}$, and the surface Brillouin zone (SBZ) corresponding to this lattice in the usual manner.[34]

Let the plane wave, described by Eq. (2), be incident on this plane of spheres. We can always write the component of its wave vector parallel to the plane of spheres as follows:

$$\mathbf{q}_\parallel = \mathbf{k}_\parallel + \mathbf{g}', \tag{8}$$

where the (reduced) wave vector $\mathbf{k}_\parallel$ lies in the SBZ and $\mathbf{g}'$ is a certain reciprocal-lattice vector. We write the wave vector of a plane wave of given wave number $q=\sqrt{\mu\epsilon}\omega/c$ and given $\mathbf{q}_\parallel=\mathbf{k}_\parallel+\mathbf{g}$ as follows:

$$\mathbf{K}^{\pm}_{\mathbf{g}} = \{\mathbf{k}_\parallel + \mathbf{g}, \pm[q^2 - (\mathbf{k}_\parallel+\mathbf{g})^2]^{1/2}\}, \tag{9}$$

where the + and − sign define the sign of the z component of the wave vector. We note that when $q^2<(\mathbf{k}_\parallel+\mathbf{g})^2$, the above defines a decaying wave; the positive sign in Eq. (9) describes a wave propagating or decaying to the right and the negative sign describes a wave propagating or decaying to the left.

We write the electric field of the incident wave in the form,

$$\mathbf{E}^{s'}_{\text{in}}(\mathbf{r}) = \sum_{i'=1}^{2}[E_{\text{in}}]^{s'}_{\mathbf{g}'i'}\exp(i\mathbf{K}^{s'}_{\mathbf{g}'}\cdot\mathbf{r})\hat{\mathbf{e}}_{i'}, \tag{10}$$

where $s'=+(-)$ corresponds to a propagating or decaying wave incident on the plane of spheres from the left (right), and $\hat{\mathbf{e}}_1$ and $\hat{\mathbf{e}}_2$ are the polar and azimuthal unit vectors, respectively, which are perpendicular to $\mathbf{K}^{s'}_{\mathbf{g}'}$. In the same manner [according to Eq. (9)] we define, for the given $\mathbf{k}_\parallel$ and q, a wave vector $\mathbf{K}^s_{\mathbf{g}}$ and the corresponding $\hat{\mathbf{e}}_i$ for any $\mathbf{g}$ and s

$=\pm$. In this way we can expand the electric-field component of an EM wave into p- and s-polarized transverse plane waves, i.e., polarized along $\hat{\mathbf{e}}_1$ and $\hat{\mathbf{e}}_2$, respectively. We note that, in the case of a decaying wave, the unit vectors $\hat{\mathbf{e}}_1$ and $\hat{\mathbf{e}}_2$ are complex but they are still orthonormal $(\hat{\mathbf{e}}_i \cdot \hat{\mathbf{e}}_j = \delta_{ij}, i,j = 1,2)$.

When the plane wave of Eq. (10) is incident on the plane from the left $(s'=+)$, the EM field at the right side of the plane is written as

$$\mathbf{E}^{+}_{\mathrm{tr}}(\mathbf{r}) = \sum_{i=1}^{2} \sum_{\mathbf{g}} [E_{\mathrm{tr}}]^{+}_{\mathbf{g}i} \exp(i\mathbf{K}^{+}_{\mathbf{g}} \cdot \mathbf{r}) \hat{\mathbf{e}}_i, \quad z > 0, \tag{11}$$

with

$$[E_{\mathrm{tr}}]^{+}_{\mathbf{g}i} = [E_{\mathrm{in}}]^{+}_{\mathbf{g}'i} \delta_{\mathbf{g}\mathbf{g}'} + [E_{\mathrm{sc}}]^{+}_{\mathbf{g}i} = \sum_{i'} Q^{I}_{\mathbf{g}i;\mathbf{g}'i'} [E_{\mathrm{in}}]^{+}_{\mathbf{g}'i'}. \tag{12}$$

The $\mathbf{Q}^I$ matrix appearing in Eq. (12) is the transmission matrix of the plane of spheres and along with other relevant scattering matrices can be found in Ref. 34. In order to find the EM force exerted on a small sphere placed at the right side of the plane of spheres, the field of Eq. (12) must be expressed as a sum of vector spherical waves incoming to the sphere in the manner of Eq. (3). Then, the EM force is calculated by means of Eqs. (6) and (7).

III. VAN DER WAALS–CASIMIR FORCE

Recently, there has been significant theoretical effort in developing methods for the calculation of the VDWC forces between macroscopic bodies, which are based on rigorous electrodynamic techniques.[39–42] Here, we present a relatively simpler approach for the VDWC forces among a finite number of macroscopic spheres than that described in Ref. 39. The VDWC forces for an array of spheres are calculated similar to the optical forces, i.e., by means of Eqs. (6) and (7) for each sphere. However, for the case of the VDWC forces, the EM field entering Eq. (7) is the vacuum zero-point fluctuating field (for $T=0$) or the thermal field $(T \neq 0)$ emitted from all spheres. The time correlation function $\langle E_i(\mathbf{r},t) E_j(\mathbf{r},t) \rangle_t$ contained in Eq. (7) is calculated within the framework of fluctuational electrodynamics,[43,44] namely from,[45]

$$\langle E_i(\mathbf{r},t) E_j(\mathbf{r},t) \rangle_t = \mathrm{Re}\left[\int_0^{\infty} \frac{d\omega}{2\pi} W^{EE}_{ij}(\mathbf{r},\mathbf{r};\omega) \right]. \tag{13}$$

The quantity $W^{EE}_{ij}(\mathbf{r},\mathbf{r};\omega)$ is the cross-spectral correlation function for the electric field. For a system at thermal equilibrium, i.e., the scatterer, the surrounding medium, and its neighboring scatterers at the same temperature T, W_{ij} is provided by the fluctuation-dissipation theorem,[46]

$$W^{EE}_{ij}(\mathbf{r},\mathbf{r};\omega) = 4\omega \mu_h \mu_0 c^2 \ \mathrm{Im}\ G^{EE}_{ij}(\mathbf{r},\mathbf{r};\omega) \hbar\omega \times \left[1 + \frac{1}{\exp(\hbar\omega/k_B T) - 1} \right], \tag{14}$$

where $\hbar$ is the reduced Planck constant, k_B is the Boltzmann constant, and $G^{EE}_{ij}(\mathbf{r},\mathbf{r}';\omega)$ is the component of the electrodynamic Green's tensor G_{ij}, which provides the electric field at $\mathbf{r}$ due to an electric dipole source at $\mathbf{r}'$. The time correlation function $\langle H_i(\mathbf{r},t) H_j(\mathbf{r},t) \rangle_t$ for the magnetic field is similar to Eq. (13) with W^{EE}_{ij} substituted by

$$W^{HH}_{ij}(\mathbf{r},\mathbf{r};\omega) = 4\omega \epsilon_h \epsilon_0 c^2 \ \mathrm{Im}\ G^{HH}_{ij}(\mathbf{r},\mathbf{r};\omega) \hbar\omega \times \left[1 + \frac{1}{\exp(\hbar\omega/k_B T) - 1} \right]. \tag{15}$$

The EM field in Eq. (13) stems from the fluctuating vacuum/thermal fields emitted from all neighboring spheres (denoted by the index n), i.e.,

$$E_i(\mathbf{r},t) = \sum_{n=1}^{N} E_i(\mathbf{r}_n,t), \tag{16}$$

where $\mathbf{r}_n = \mathbf{r} - \mathbf{R}_n$. The time correlation function for the electric field of Eq. (13) for the case of N thermal sources is written as

$$\begin{aligned} \langle E_i(\mathbf{r},t) E_j(\mathbf{r},t) \rangle_t &= \Big\langle \sum_{n=1}^{N} \sum_{n'=1}^{N} E_i(\mathbf{r}_n,t) E_j(\mathbf{r}_{n'},t) \Big\rangle_t \\ &= \sum_{n=1}^{N} \langle E_i(\mathbf{r}_n,t) E_j(\mathbf{r}_n,t) \rangle_t \\ &\quad + \sum_{n \neq n'} \langle E_i(\mathbf{r}_n,t) E_j(\mathbf{r}_{n'},t) \rangle_t, \end{aligned} \tag{17}$$

When the spheres are made from different materials, they can be viewed as totally incoherent thermal sources. In this case, the second term of Eq. (17) vanishes,

$$\langle E_i(\mathbf{r}_n,t) E_j(\mathbf{r}_{n'},t) \rangle_t \cong \langle E_i(\mathbf{r}_n,t) \rangle_t \langle E_i(\mathbf{r}_{n'},t) \rangle_t = 0, \tag{18}$$

since for the vacuum fluctuations the time-averaged field vanishes, i.e., $\langle E_i(\mathbf{r}_{n'},t) \rangle_t = 0$. The same holds for the corresponding time averages of the magnetic field $H_i(\mathbf{r},t)$. We note that Eq. (18) can also be justified in the case where the spheres are made from the same material for frequencies away from resonant states such as the surface-plasmon states in metals. In the latter case, the excitation of surface plasmons in each sphere could lead to a collective emission/scattering from all spheres. However, when it comes to the calculation of VDWC forces, an integral over frequency spectrum is needed [see Eq. (13)] and, therefore, the frequency regions, where the approximation of Eq. (18) is not entirely justified, do not influence significantly the final result. Due to Eq. (18), Eq. (14) becomes

$$W^{EE}_{ij}(\mathbf{r},\mathbf{r};\omega) = 4\omega \mu_h \mu_0 c^2 \hbar\omega \times \left[1 + \frac{1}{\exp(\hbar\omega/k_B T) - 1} \right] \mathrm{Im} \sum_{n=1}^{N} G^{s;EE}_{ij}(\mathbf{r}_n,\mathbf{r}_n;\omega), \tag{19}$$

where $G^{s;EE}_{ij}(\mathbf{r}_n,\mathbf{r}_n;\omega)$ is the EM Green's tensor for a *single* sphere; explicit relations can be found elsewhere.[47] We note

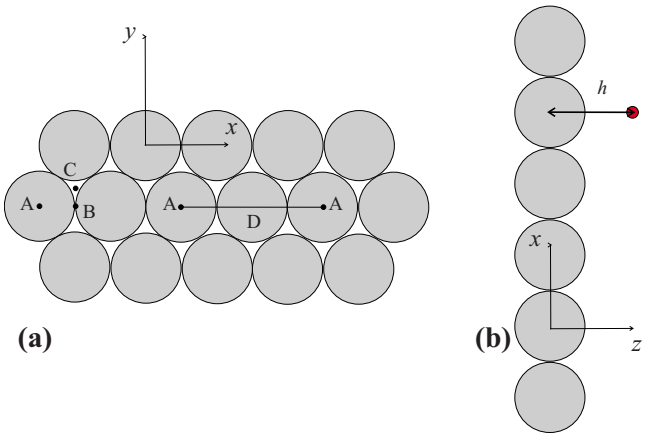

FIG. 1. (Color online) (a) Top view a monolayer of close-packed spheres. (b) Side view of the monolayer and the test sphere.

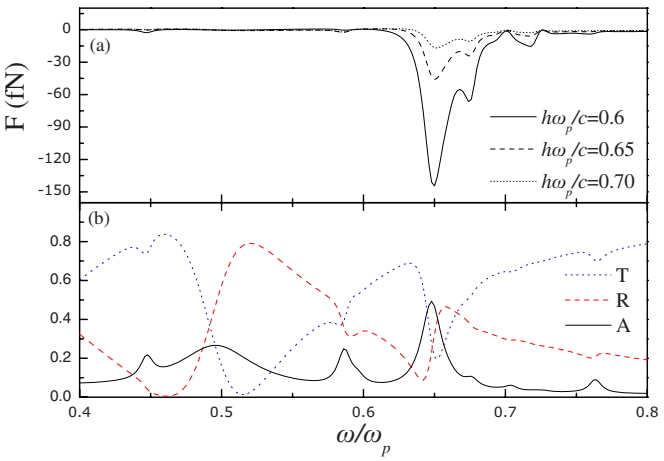

FIG. 2. (Color online) (a) Optical force exerted on a test polystyrene nanoparticle (ϵ_t=2.56 and S_t=0.05c/ω_p) placed above the center [$\mathbf{r}_t$=(0,0,h)—point A of Fig. 1] of a plasmonic (gold, $\hbar\omega_p$=8.99 eV, and $\hbar\gamma$=0.07 eV) nanosphere belonging to a (hexagonal) monolayer of close-packed (S_m=0.5c/ω_p) spheres at various distances h from the center of the sphere. The monolayer is illuminated by a normally incident plane wave of intensity I=5 $\times 10^{11}$ W/m^2 polarized along the x axis, which coincides with the direction of one of the 2D primitive vectors of the hexagonal lattice of the monolayer. (b) Transmittance (T), reflectance (R), and absorbance (A) spectra of light incident normally on the monolayer of spheres described above.

that Eq. (19) is a far easier means to calculate W_{ij}^{EE} since it only involves the calculation of the single sphere Green's tensor G_{ij}^{s} and not the full Green's tensor G_{ij}. The latter includes all the multiple-scattering processes in which the vacuum/thermal field undergoes,[47] which constitute an unnecessary complication to our problem since the spheres are considered incoherent.

A final note is done on the integral of Eq. (13). Due to the analytic properties of the EM Green's tensor, we can perform the integral over the imaginary frequency axis rather than the real frequency axis. The VDWC force spectrum for imaginary frequencies is a much smoother function than the corresponding integrand for real frequencies.[42,48]

IV. RESULTS

We consider a monolayer of close-packed plasmonic (metallic) spheres, i.e., the underlying 2D lattice is hexagonal [see Fig. 1(a)]. Recent advances in fabrication allow for the realization of well defined ordered arrays of such particles.[49,50] Since the spheres are in a close-packed arrangement, nonlocal effects come into play.[51,52] Therefore, we have made use of a nonlocal dielectric function for the metallic spheres, according to the hydrodynamic model.[53,54] Namely, within the hydrodynamic model, the transverse ϵ_T and longitudinal ϵ_L dielectric functions are given by

$$\epsilon_T(\omega) = 1 - \frac{\omega_p^2}{\omega(\omega + i\gamma)} \tag{20}$$

$$\epsilon_L(q,\omega) = 1 - \frac{\omega_p^2}{\omega^2 - \beta q^2 + i\omega\gamma}, \tag{21}$$

where ω_p is the bulk plasma frequency of the metal and γ is the loss factor. $\beta = \frac{3}{5}v_F^2$, where v_F is the Fermi velocity of the metal. Equation (20) is the ordinary Drude dielectric function, which is widely used to describe metals within the local response approximation. We have chosen $\hbar\omega_p$=8.99 eV and $\hbar\gamma$=0.07 eV, which are suitable parameters for gold nanospheres.[55] The Fermi velocity of gold is taken v_F =1.39 cm/sec (Ref. 56). The radius of the plasma (gold) spheres is taken to be $S_m\omega_p/c$=0.5. In order to probe the trapping features of the above plasmonic nanostructure, we place a much smaller (compared to the metallic spheres of the monolayer) dielectric (ϵ_t=2.56—polystyrene) sphere of radius $S_t\omega_p/c$=0.05. The small size of this test sphere ensures the applicability of the theory of Sec. II, which does not take into account the presence of the test sphere in the calculation of the total EM field incident on this sphere. The small size of the dielectric sphere as compared to the characteristic length of the nanostructure renders the inclusion of the light multiple-scattering processes between the sphere and the nanostructure, an unnecessary complexity to our problem. This physical picture is analogous to the case of atom trapping within an optical lattice; there, the size of an atom is much smaller than the characteristic scale of the optical potential lattice.

Figure 2(a) shows the spectrum of the optical force acting on the dielectric test sphere located exactly above the center of a metallic nanosphere [point A of Fig. 1(a)] and for different values of the separation h [see Fig. 1(b)] from the monolayer. The monolayer is illuminated from the left with a normally incident plane wave of intensity I=5 $\times 10^{11}$ W/m^2 and polarization parallel along the x axis, which coincides with the direction of one of the 2D primitive vectors of the hexagonal lattice of the monolayer. The sphere is placed on the right side of the monolayer and, therefore, the optical force is exerted from the transmitted wave [Eqs. (11) and (12)]. Figure 2(a) depicts the z component of the force while the other components are zero due to symmetry. Figure 2(b) depicts the transmittance, reflectance, and absorbance spectra of normally incident light on the nanostructure.

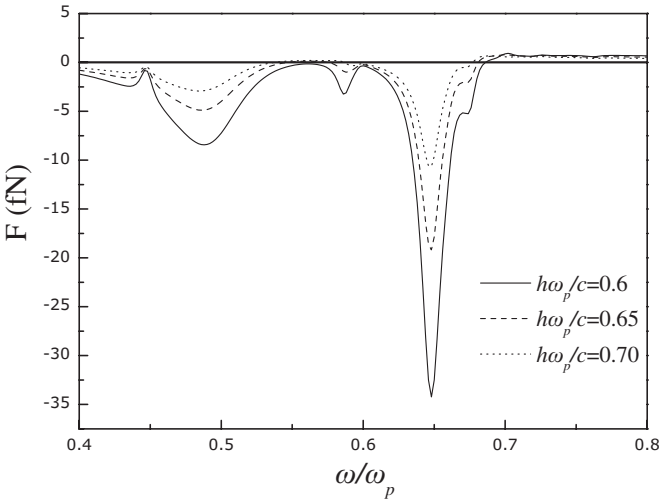

FIG. 3. The same as Fig. 2(a) but for a different position of the test sphere, i.e., $\mathbf{r}_t=(S_m,0,h)$—point B of Fig. 1.

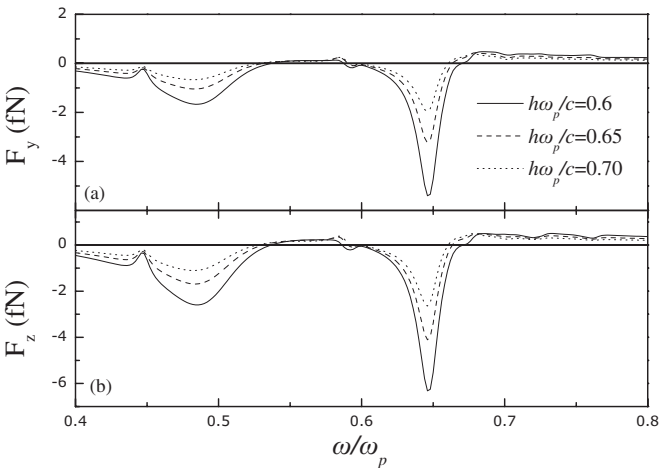

FIG. 4. Spectra of the y and z components of the optical force exerted on the test polystyrene nanoparticle when the latter is located at $\mathbf{r}_t=(S_m,\sqrt{3}/6,h)$—point C of Fig. 1.

By observing Fig. 2(a) we can infer that the optical force acting on the test sphere is generated primarily by the gradient of the near-field optical landscape near the nanostructure since the force decreases rapidly as the test particle moves away from the nanostructure. Also, the force is attractive as expected from the decaying nature of the near field away from the nanostructure. Had the force been the result of radiation pressure exerted by propagating waves, it would be repulsive and independent of the distance h from the monolayer. We also observe that the optical force exhibits a main dip at $\omega/\omega_p=0.65$ and an accompanying structure up to $\omega/\omega_p<0.72$. The force peak corresponds to a maximum of the absorbance/reflectance curves.

For a relatively dilute monolayer of nontouching plasmonic spheres of this size, the structure in the absorbance curves is a result of the excitation of dipolar surface plasma modes at the spheres, occurring at $\omega_1/\omega_p=1/\sqrt{3}\approx 0.577$. Namely, the surface plasmons of each sphere interact with the corresponding modes of neighboring spheres in a tight-binding fashion, resulting in a frequency band of states within which light extinction (absorption and scattering) is enhanced.[57,58] Higher multipolar surface plasmons occurring around $\omega_l/\omega_p=\sqrt{l/(2l+1)}$, where $l=1,2,3,\cdots$, can also be excited leading to a secondary structure in the absorption spectrum.[57,58] However, as the sphere size and/or the spheres come closer (denser structure), higher multipolar surface modes may dominate the absorbance spectrum. For the case of a close-packed array (touching spheres) such as the one considered here, the interaction among surface plasmons of neighboring spheres is maximum, leading to large frequency shifts and broadening of the various surface-plasmon bands; the latter are formed away from the single sphere surface plasmons as it is evident from Fig. 2(b). We note that, since metal covers about 78.5% of the 2D space in a close-packed arrangement of spheres, the optical response of such an array can be alternatively described as that of a homogeneous metal containing air holes (cavities) of nanometer scale.[52,59]

Figure 3 is the same as Fig. 2 but for the point B of Fig. 1(a) (due to symmetry, the x and y components are again zero). At this point, the sphere lies above the touching point of two spheres, at a distance h from the layer. We observe that the absolute value of the optical force assumes at least three times smaller values with respect to Fig. 2(a). The main force minimum lies, again, at $\omega/\omega_p=0.65$. For frequencies $\omega/\omega_p>0.7$ the force becomes repulsive and practically independent of the distance h. This means that the main contribution to the optical force for $\omega/\omega_p>0.7$ comes from the radiation pressure rather than from the gradient of the near-field intensity. One also observes additional dips at $\omega/\omega_p\approx 0.49$ and at $\omega/\omega_p\approx 0.58$, which are not present in Fig. 2(a). These peaks correspond, more or less, to peaks of the absorbance spectrum in Fig. 2(b). This might be an evidence that the absorption process takes place primarily in the space among the spheres. Similar features are evident for the optical force corresponding to point C of Fig. 1(a) (Fig. 4). For symmetry reasons, the x component for point C is zero for this point. We also note that the optical force assumes smaller values than in Figs. 2 and 3.

Next, we examine the possibility of trapping the test particle with optical means. Therefore, we choose to study the spatial dependence of the optical force for a particular frequency, namely for $\omega/\omega_p=0.65$. The latter frequency corresponds to the main dip of the force spectra of Figs. 2–4. However, for a comprehensive treatment of the problem, we need to take into account the VDWC forces acting on the test sphere from the plasmonic nanospheres of the monolayer. By applying the formalism of Sec. III, we have calculated the VDWC force between a single plasmonic nanoparticle of the monolayer and the test polystyrene sphere, as a function of their center-to-center distance (see Fig. 5). We note that, according to Eq. (13) (a similar equation is obeyed by the magnetic field), we need to integrate the corresponding cross-spectral correlation functions W_{ij}^{PP}, where $P=E,H$ over the positive-frequency spectrum. As a result, for the polystyrene nanosphere, we have made use of an experimentally obtained dielectric function,[48] which is generally frequency dependent (it contains contributions from the UV region). As it is evident from Fig. 5, the VDWC force is attractive and it decays very rapidly with distance (the power exponent is

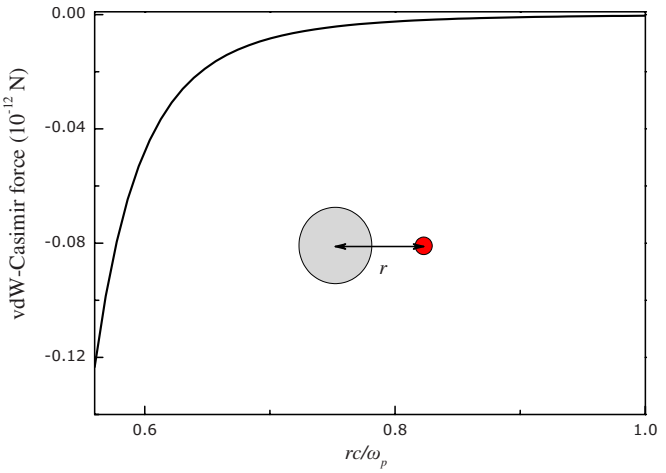

FIG. 5. (Color online) VDWC force between a plasmonic (gold, $\hbar\omega_p$=8.99 eV, $\hbar\gamma$=0.07 eV, and $S_m=0.5c/\omega_p$) and polystyrene nanosphere (ϵ_t given by Ref. 48 and $S_t=0.05c/\omega_p$).

around 9.6). Due to this rapid decrease, in order to obtain the total VDWC acting on the polystyrene test sphere from the monolayer of spheres, the contributions from neighboring spheres are vectorially added in a pairwise fashion.

Figure 6 shows the optical and VDWC forces along the line D of Fig. 1(a), for different distances h from the monolayer. As stated above, the optical force is calculated for frequency ω/ω_p=0.65. The y component of both forces is zero. It is evident that there exist several points where the forces are zero. The optical force contains more roots along the given line. However, at symmetric points within the unit cell (center of a sphere or touching point between two spheres) both forces become zero and the test particle can be trapped within a plane parallel to the monolayer (transverse trapping). For more intense laser beams, the optical force can render the VDWC force negligible and the particle can po-

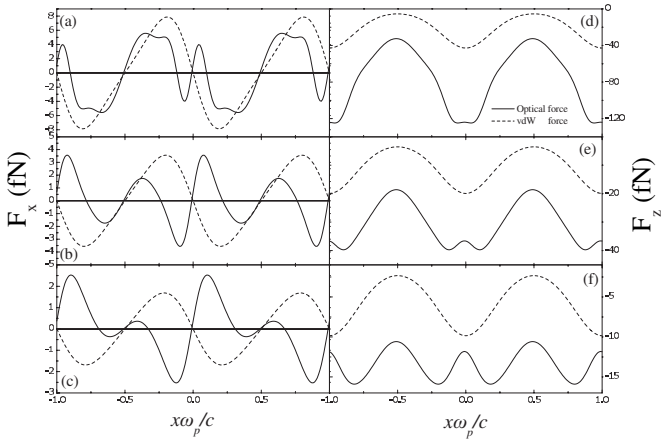

FIG. 6. Optical (solid lines) and VDWC (broken lines) forces exerted on a polystyrene nanoparticle near a monolayer of plasmonic spheres along the direction $\mathbf{r}_t=(x,0,h)$ with $-2S_m \leq x \leq 2S_m$ [line D of Fig. 1(a)] and different distances from the monolayer: [(a) and (d)] $h=0.6c/\omega_p$, [(b) and (e)] $h=0.65c/\omega_p$, and [(c) and (f)] $h=0.7c/\omega_p$. The left figures depict the x component while the right ones depict the z component.

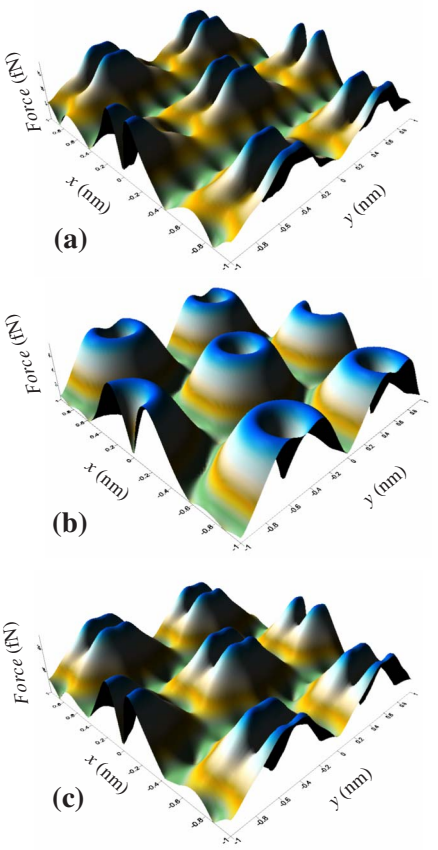

FIG. 7. (Color online) Magnitude of the parallel component of (a) the optical force, (b) the VDWC force, and (c) the total (optical+VDWC) force within the area $-2S_m<x,y<2S_m$ at a distance $h=0.6c/\omega_p$ from the plane of spheres.

tentially be trapped at all of the zeroes of the optical force. However, for the given laser intensity, the VDWC is comparable to the optical force. Figures 6(d)–6(f) depict the z component of both forces. It is evident that both force components are attractive and, therefore, cannot offer vertical trapping of the particle. However, for distances smaller than 1 nm, the atomic structure of the spheres becomes evident and a more accurate description of the VDWC interaction possibly requires a microscopic treatment, which accounts for Born repulsive forces stemming from exchange and electrostatic interactions.[60] The latter forces have to be taken into account to estimate the equilibrium z distance from the monolayer. Furthermore, a microscopic treatment of the VDWC interaction would also take into account surface phenomena such as charge redistribution and surface reconstruction, which become significant for very small separations.

Figure 7 depicts the magnitude of the transverse component of the (a) optical, (b) VDWC, and (c) total (optical +VDWC) force within the xy plane at a distance $h=0.6c/\omega_p$ from the monolayer. We observe that the optical force exhibits a much more complicated landscape than the VDWC force. It is also evident that optical force contains more zeroes (trapping points), which can be located at nonsymmetric points as well. This is due to the fact that the optical force depends on the polarization vector of the incident plane wave. The VDWC force becomes zero at the

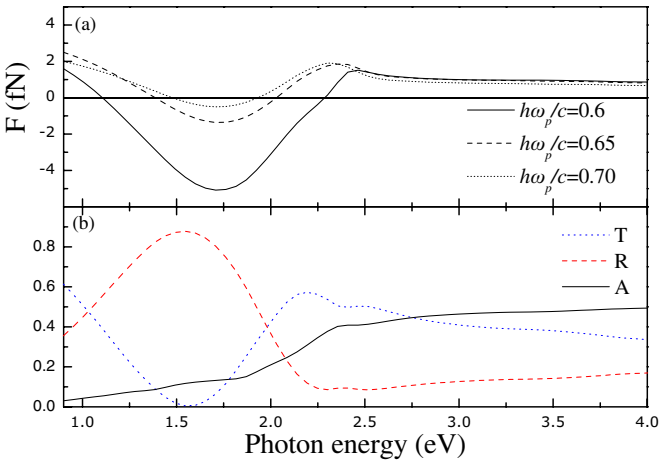

FIG. 8. (Color online) The same as Fig. 2 but for an experimental dielectric function (Ref. 61) describing the optical response of the gold nanospheres.

sphere centers and at points in the space among the spheres of the monolayer. However, for the given laser intensity, the VDWC force does not seem to affect dramatically the trapping points, since the total force landscape does not seem to differ significantly from that of the pure optical force.

The results presented until now are for a monolayer of gold nanospheres described by a Drude-type dielectric function. It is well known that this type of dielectric function takes into account only the free-electron excitations (plasmons) of a metal, neglecting other important contributions such as the interband transitions. However, since there are no analytic nonlocal dielectric functions beyond the Drude-type one, the above contributions have not been considered in the results presented so far. In order to study the effect of interband transitions, we have recalculated Fig. 2 for gold spheres whose dielectric function is taken from experiment (see Fig. 8).[61] Note that, although the contribution of the interband transitions is included in an experimental dielectric function, the latter is still an approximation to our problem since a local dielectric function is being used and the close-packed arrangement of spheres requires a nonlocal one.[52] From Fig. 8 it is evident that the optical force is, again, significant around the (dipolar) surface-plasmon resonant band manifested as a peak in the reflectance curve. Naturally, the force is attractive due to the dominant role of the decaying near-field components of the scattered EM field. As the distance from the monolayer of spheres increases, the contribution of the near field diminishes in favor of the far field (propagating components, which result in a repulsive force), leading to a narrower spectrum of attractive force. The fine structure appearing in all spectra of Fig. 2 and stems from higher multipole surface plasmons is evidently lost within the absorption tail of the interband transitions.[62] The optical force of Fig. 8 assumes much smaller values than the corresponding one of Fig. 2. This implies that a higher radiation intensity is needed (than that assumed in Figs. 2 and 8) in order to overcome the VDWC forces. However, this may be only approximately correct due to the local nature of the experimental dielectric function used in Fig. 8.

Finally, we address briefly the issue of the thermal motion of the test particle. We know that for stable optical confinement of the particle, the optical potential trap should be deep enough to prevent escape of the particle due to its thermal motion. If we estimate the energy needed for a particle to escape from the optical trap reported here, as the area (work) below the force curve between two consecutive zeroes (see Fig. 6), then this is of the order of one thousandth of the thermal energy k_BT. Therefore, for an experimental demonstration of the optical trapping, low temperatures or higher laser intensities are prerequisites.

V. CONCLUSIONS

We have presented a formalism for the calculation of the optical forces acting on particle placed next to an illuminated plane of plasmonic nanospheres. The formalism is based on exact accounting of the multiple-scattering of the EM field within the plane of spheres and application of the Maxwell stress tensor for the determination of the optical force on the particle. The optical force is strong within frequency bands corresponding to surface-plasmon excitations of the plasmonic spheres. Within these frequency bands, the optical force stems from the gradient of the optical near field generated by the scattering of incident light on the nanostructure. Along with the optical force, we have calculated the VDWC force exerted on the test particle from the plane of spheres. For high enough laser intensities, the optical forces become comparable to the VDWC leading to the trapping of the particle in a plane parallel to the monolayer of spheres. However, much higher intensities are needed to overcome the thermal motion of the particle.

*vyannop@upatras.gr

[1] A. Ashkin, Phys. Rev. Lett. **24**, 156 (1970).
[2] A. Ashkin, Phys. Rev. Lett. **25**, 1321 (1970).
[3] A. Ashkin, J. M. Dziedzic, J. E. Bjorkholm, and S. Chu, Opt. Lett. **11**, 288 (1986).
[4] D. G. Grier, Nature (London) **424**, 810 (2003).
[5] K. Dholakia and P. Reece, Nanotoday **1**, 18 (2006).
[6] A. Ashkin, Proc. Natl. Acad. Sci. U.S.A. **94**, 4853 (1997).
[7] T. Iida and H. Ishihara, Phys. Rev. Lett. **90**, 057403 (2003).
[8] L. Novotny, R. X. Bian, and X. S. Xie, Phys. Rev. Lett. **79**, 645 (1997).
[9] K. Okamoto and S. Kawata, Phys. Rev. Lett. **83**, 4534 (1999).
[10] P. C. Chaumet and M. Nieto-Vesperinas, Phys. Rev. B **62**, 11185 (2000).
[11] M. M. Burns, J. M. Fournier, and J. A. Golovchenko, Phys. Rev. Lett. **63**, 1233 (1989).
[12] M. M. Burns, J. M. Fournier, and J. A. Golovchenko, Science **249**, 749 (1990).
[13] J. P. Hoogenboom, D. L. J. Vossen, C. Faivre-Moskalenko, and M. Dogterom, Appl. Phys. Lett. **80**, 4828 (2002).

[14] A. N. Rubinov, V. M. Katarkevich, A. A. Afanas'ev, and T. S. Efendiev, Opt. Commun. **224**, 97 (2003).
[15] W. M. Lee and X. C. Yuan, Appl. Phys. Lett. **83**, 5124 (2003).
[16] J. Ng, Z. F. Lin, C. T. Chan, and P. Sheng, Phys. Rev. B **72**, 085130 (2005).
[17] C. D. Mellor, T. A. Fennerty, and C. D. Bain, Opt. Express **14**, 10079 (2006).
[18] T. M. Grzegorczyk, B. A. Kemp, and J. A. Kong, Phys. Rev. Lett. **96**, 113903 (2006).
[19] M. I. Antonoyiannakis and J. B. Pendry, Phys. Rev. B **60**, 2363 (1999); Europhys. Lett. **40**, 613 (1997).
[20] V. Garcés-Chávez, D. McGloin, H. Melville, W. Sibbett, and K. Dholakia, Nature (London) **419**, 145 (2002).
[21] L. Paterson, M. P. MacDonald, J. Arlt, W. Sibbett, P. E. Bryant, and K. Dholakia, Science **292**, 912 (2001).
[22] M. P. MacDonald, L. Paterson, K. Volke-Sepulveda, J. Arlt, W. Sibbett, and K. Dholakia, Science **296**, 1101 (2002).
[23] P. J. Rodrigo, V. R. Daria, and J. Glückstad, Opt. Express **12**, 1417 (2004).
[24] R. Agarwal, K. Ladavac, Y. Roichman, G. Yu, C. Lieber, and D. Grier, Opt. Express **13**, 8906 (2005).
[25] C. Schmitz, J. Spatz, and J. Curtis, Opt. Express **13**, 8678 (2005).
[26] Y. Roichman, I. Chois, and D. G. Grier, Opt. Express **14**, 10907 (2006).
[27] Z. Lu, J. A. Murakowski, C. A. Schutz, S. Shi, G. J. Schneider, J. P. Samluk, and D. W. Prather, Opt. Express **14**, 2228 (2006).
[28] O. Toader, S. John, and K. Busch, Opt. Express **8**, 217 (2000).
[29] A. Rahmani and P. C. Chaumet, Opt. Express **14**, 6353 (2006).
[30] J. Bravo-Abad, M. Ibanescu, J. D. Joannopoulos, and M. Soljačić, Phys. Rev. A **74**, 053619 (2006).
[31] J. Ng, C. T. Chan, P. Sheng, and Z. Lin, Opt. Lett. **30**, 1956 (2005).
[32] H. Xu and M. Käll, Phys. Rev. Lett. **89**, 246802 (2002).
[33] Z. Li, M. Käll, and H. Xu, Phys. Rev. B **77**, 085412 (2008).
[34] N. Stefanou, V. Yannopapas and A. Modinos, Comput. Phys. Commun. **113**, 49 (1998); **132**, 189 (2000).
[35] J. D. Jackson, *Classical Electrodynamics* (Wiley, New York, 1975).
[36] C. F. Bohren and D. R. Huffman, *Absorption and Scattering of Light by Small Particles* (Wiley, New York, 1983).
[37] J. P. Barton and D. R. Alexander, J. Appl. Phys. **66**, 4594 (1989).
[38] A. A. R. Neves, A. Fontes, L. Y. Pozzo, A. A. de Tomaz, E. Chillce, E. Rodriguez, L. C. Barbosa, and C. L. Cesar, Opt. Express **14**, 13101 (2006).
[39] V. Yannopapas and N. V. Vitanov, Phys. Rev. Lett. **99**, 120406 (2007).
[40] V. Yannopapas, Phys. Rev. B **76**, 235415 (2007).
[41] A. Rodriguez, M. Ibanescu, D. Iannuzzi, F. Capasso, J. D. Joannopoulos, and S. G. Johnson, Phys. Rev. Lett. **99**, 080401 (2007).
[42] A. Rodriguez, M. Ibanescu, D. Iannuzzi, J. D. Joannopoulos, and S. G. Johnson, Phys. Rev. A **76**, 032106 (2007).
[43] G. Agarwal, Phys. Rev. A **11**, 253 (1975).
[44] S. M. Rytov, Yu. A. Kravtsov, and V. I. Tatarskii, *Principles of Statistical Radiophysics*, Elements of Random Fields Vol. 3 (Springer, Berlin, 1989).
[45] K. Joulain, J.-P. Mulet, F. Marquier, R. Carminati, and J.-J. Greffet, Surf. Sci. Rep. **57**, 59 (2005).
[46] H. B. Callen and T. A. Welton, Phys. Rev. **83**, 34 (1951).
[47] V. Yannopapas and N. V. Vitanov, Phys. Rev. B **75**, 115124 (2007).
[48] V. A. Parsegian, *Van der Waals Forces* (Cambridge University Press, Cambridge, 2006).
[49] A. Taleb, V. Russier, A. Courty, and M. P. Pileni, Phys. Rev. B **59**, 13350 (1999).
[50] N. Pinna, M. Maillard, A. Courty, V. Russier, and M. P. Pileni, Phys. Rev. B **66**, 045415 (2002).
[51] C. Tserkezis, G. Gantzounis, and N. Stefanou, J. Phys.: Condens. Matter **20**, 075232 (2008).
[52] V. Yannopapas, J. Phys.: Condens. Matter **20**, 325211 (2008).
[53] F. Forstmann and R. P. Gerhardts, *Festkörperprobleme*, Advances in Solid State Physics Vol. 22 (Vieweg, Braunschweig, 1982), p. 291.
[54] R. Ruppin, Phys. Rev. B **11**, 2871 (1975).
[55] V. Yannopapas, Phys. Rev. B **73**, 113108 (2006).
[56] N. W. Ashcroft and N. D. Mermin, *Solid State Physics* (Saunders, Fort Worth, 1976).
[57] N. Stefanou and A. Modinos, J. Phys.: Condens. Matter **3**, 8135 (1991); **3**, 8149 (1991).
[58] G. Gantzounis, N. Stefanou, and V. Yannopapas, J. Phys.: Condens. Matter **17**, 1791 (2005).
[59] G. Gantzounis and N. Stefanou, Phys. Rev. B **74**, 085102 (2006); J. Phys.: Condens. Matter **20**, 015202 (2008).
[60] J. X. Lu and W. H. Marlow, Phys. Rev. A **52**, 2141 (1995); J. X. Lu, W. H. Marlow, and V. Arunachalam, J. Colloid Interface Sci. **181**, 429 (1996).
[61] R. B. Johnson and R. W. Christy, Phys. Rev. B **6**, 4370 (1972).
[62] V. Yannopapas, A. Modinos, and N. Stefanou, Opt. Quantum Electron. **34**, 227 (2002).